25 YEARS

jmr Journal of MATERIALS RESEARCH

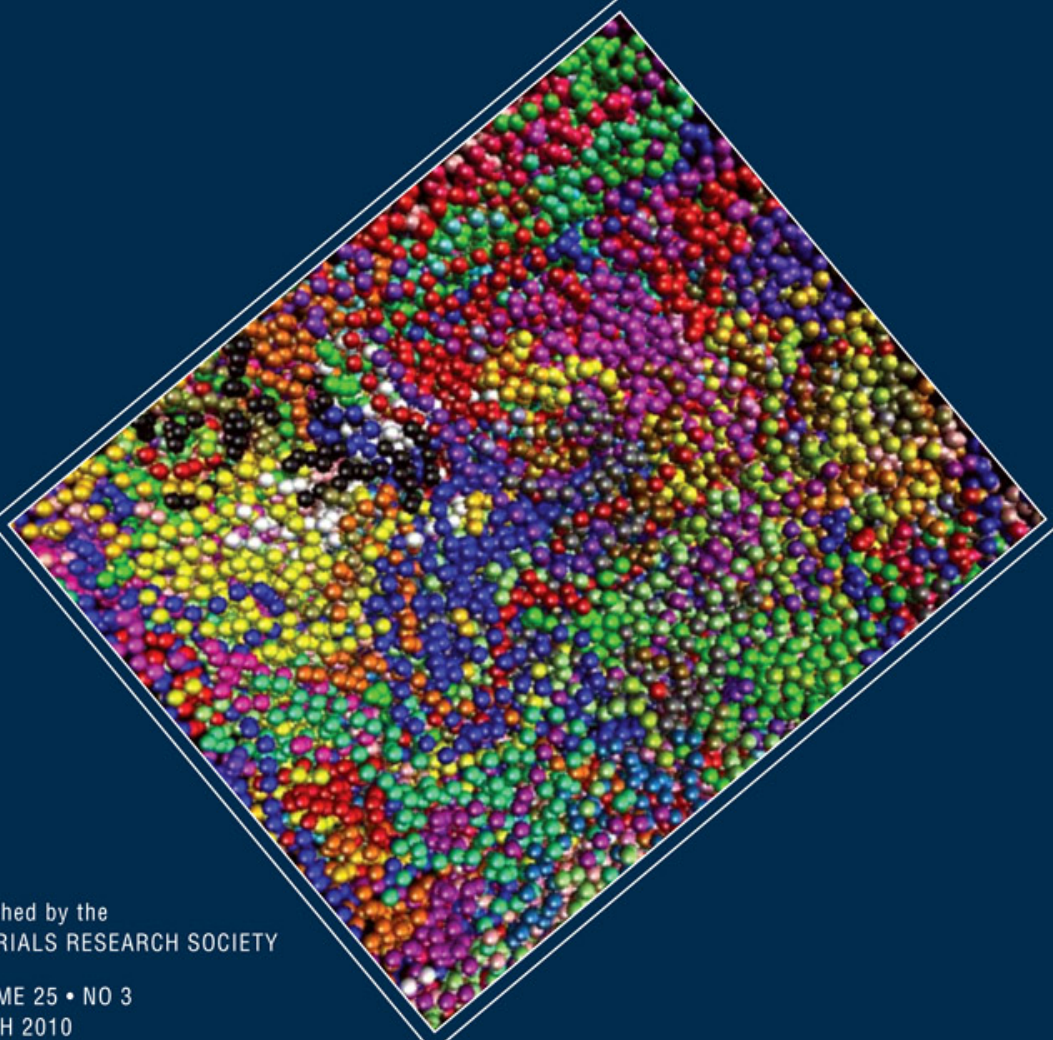

Published by the
MATERIALS RESEARCH SOCIETY

VOLUME 25 • NO 3
MARCH 2010

Thermomechanical properties dependence on chain length in bulk polyethylene: Coarse-grained molecular dynamics simulations

Junhua Zhao, Shijo Nagao, and Zhiliang Zhang[a)]
NTNU Nanomechanical Lab, Department of Structural Engineering, Norwegian University of Science and Technology (NTNU), 7491 Trondheim, Norway

(Received 22 June 2009; accepted 1 September 2009)

Mechanical and thermodynamical properties of bulk polyethylene have been scrutinized using coarse-grained (CG) molecular dynamics simulations. Entangled but cross-link-free polymer clusters are generated by the semicrystalline lattice method for a wide range chain length of alkane modeled by CG beads, and tested under compressive and tensile stress with various temperature and strain rates. It has been found that the specific volume and volumetric thermal expansion coefficient decrease with the increase of chain length, where the specific volume is a linear function of the bond number to all bead number ratios, while the thermal expansion coefficient is a linear rational function of the ratio. Glass-transition temperature, however, does not seem to be sensitive to chain length. Yield stress under tension and compression increases with the increase of the bond number to all bead number ratio and strain rate as well as with decreasing temperature. The correlation found between chain length and these physical parameters suggests that the ratio dominates the mechanical properties of the present CG-modeled linear polymer material.

I. INTRODUCTION

Glassy polyethylene (PE) is one of the most fundamental polymer materials that have been widely applied to various fields in modern industry. The outstanding combination of physical and mechanical properties of the material attracts many materials engineers, chemists, and physicists.[1–3] Great efforts have been made for decades to clarify these properties in both theoretical and experimental studies. Hanscomb and Kaahwa[4,5] reported the high electrical conductivity of PE terephthalate at elevated temperature. Donald et al.[6,7] investigated strain hysteresis under tensile stress, and found that cracklike defects (crazes) appear within the apparent elastic strain; crazes bridged by fibrils are initiated with increasing load, and macroscopic fracture occurs immediately after the failure of these fibrils.[6,7] G'Sell et al.,[8] Arruda and Boyce,[9] and Boyce et al.[10] independently provided video-recorded tension and compression tests for various amorphous polymers, showing that typical stress–strain response exhibits normal viscoelasticity under the initial loading process, followed by strain softening after yielding, and then followed by strain hardening. Recently, Melick et al.[11] revealed that cross-linking network density in polymer materials plays an important role in the mechanisms of the strain hardening. Our previous work[12] discovered that the constitutive properties of spherical polymer microsized particles vary according to their size, confirmed by the high-resolution depth-sensing nanoindentation technique equipped with a flat-punch diamond indenter.[12] Phenomenological explanations by continuum mechanics are not sufficient for the above experimental findings since the mechanisms of those phenomena originate in atomistic or molecular structures of polymers. Understanding the atomistic origins is highly required to control their mechanical and thermal properties.

Early theoretical studies have successfully revealed certain key issues, while the introduced hypotheses and simplifications limit their applicabilities.[13–16] Recent developments of molecular dynamics (MD) simulation have opened the door for understanding and predicting the mechanical and physical properties of various polymer materials.[17–21] Zhang[22] studied the propagation of solitary waves in PE by all-atoms (AA) calculations. Capaldi et al.[23] investigated the mechanical behavior of the material by the united atoms (UA) method under dynamic compression. Nielsen et al.[24] calculated surface tension in PE by coarse-grained (CG) molecular model, which considerably reduces the amount of numerical computing required in the MD simulations.[25,26] Müller-Plathe's group reported many interesting properties of different polymers (e.g., thermal conductivity, chain stiffness, and so on) by the three MD methods.[27–29] Theodoru and Fermeglia investigated the multiscale modeling for polymer systems using the three methods and Monte Carlo (MC) method.[30–32] These three types of MD models with respective empirical pair potentials

[a)]Address all correspondence to this author.
e-mail: zhiliang.zhang@ntnu.no
DOI: 10.1557/JMR.2010.0061

give thermodynamically consistent results,[24–26,30–32] and indeed help us to better understand the polymer materials from the atomistic level of their molecular structures.

In this work, we adopt the multiscale CG method[24] to investigate the mechanical and thermodynamical properties of bulk glassy PE, which is modeled as entangled but cross-link-free CG chains generated by the semicrystalline lattice method.[33] The CG method works satisfactorily, which has been validated by comparing with AA MD simulations.[24] In particular, the effects of molecular length on equilibrium bulk density, thermal expansion coefficient, and glass-transition temperature (T_g) are systematically calculated as a function of N_{cl} (number of carbons in one chain) from hexane ($N_{cl} = 6$) to hexactane ($N_{cl} = 600$). The mechanical properties dependence on chain length and temperature as well as strain rate are investigated in detail under uniaxial tension and compression from nonane ($N_{cl} = 9$) to nonactane ($N_{cl} = 900$). The observed clear correlations between N_{cl} and those material parameters suggest that the bond number to all bead number ratios determine the mechanical properties of the present CG-modeled linear polymer material.

II. COMPUTATIONAL METHODS

The bulk structure of PE can be modeled by entangled polymer chains. To generate computer simulation cluster, we use the semicrystalline lattice method,[33] which use the face-centered cubic (fcc) diamond structure as a template to carbon backbones of entangled polymers. Because of the same quadruple covalent bonds of carbons in both diamond and PE, the bond angles are similar, and thus the generated dense semicrystalline polymers are expected to be close to equilibrium state. Linear polymer molecules are generated by the random walk process on the diamond lattice without explicit bias or guidance, except for one-step-forward collision-check to avoid obvious self-crossing. Instead, simple backtracking along the last several growth steps are used in case of both intra- and intermolecular crossing, and retry random walk until the molecule reaches the required chain length. This random walk process is found to be sufficient to achieve realistic density of linear polyethylene cluster. The generated chains of carbons are then replaced with CG beads, so that each CG bead represents the mass center of three monomers. According to Nielsen et al.[24] and Shinoda et al.,[34] CG potentials are set (see Table I) for two kinds of beads: terminal (T) bead and middle (M) ones of a molecular chain represent CH_3–CH_2–CH_2–, and –CH_2–CH_2–CH_2–, respectively (see Fig. 1).

Because the bulk density, thermal expansion coefficient, and T_g are obtained in the equilibrium MD simulations, these initial structures are generated in a $5 \times 5 \times 5$ nm^3 cubic space with three-dimensional periodic boundary conditions that can be used to calculate the three parameters.

TABLE I. Potential functions and corresponding parameters of the coarse-grained method,[24,34] in which T is a CH_3–CH_2–CH_2– bead and M is a –CH_2–CH_2–CH_2– bead.

Interaction	Form	Parameters
Bond	$E = \frac{1}{2}k_b(r_b - r_0)^2$	k_b = 6.96 (TT), k_b = 6.16 (TM, MM) kcal/mol Å^2 r_0 = 3.65 (TM), r_0=3.64 (MM) Å
Angle	$E = \frac{1}{2}k_\theta(\theta - \theta_0)^2$	k_θ = 1.09 (TMT), k_θ = 1.19 (TMM, MMM) kcal/mol θ_0 = 175.5 (TMT), θ_0 = 175 (TMM), θ_0 = 173 (TMM) degree
Nonbonded	$E = \left(\frac{27\varepsilon}{4}\right)\left[\left(\frac{\sigma}{r}\right)^9 - \left(\frac{\sigma}{r}\right)^6\right]$	ε = 0.469 (TT), ε= 0.444 (TM), ε = 0.42 (MM) kcal/mol σ = 4.585 (TT), σ = 4.5455 (TM), σ = 4.506 (MM) Å r_c = 15 Å (truncation radius)

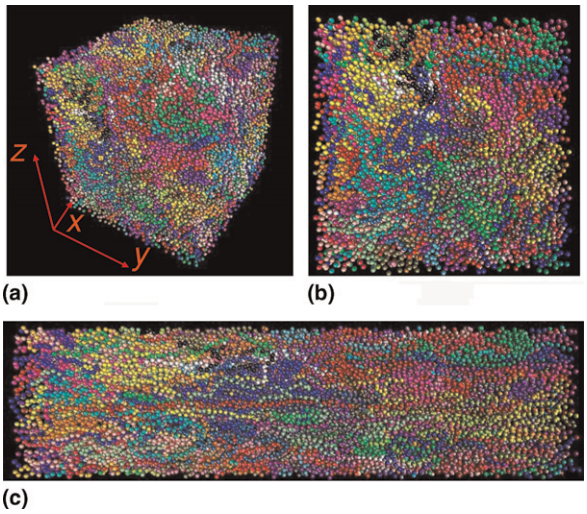

FIG. 1. Deformation sequence of PE consisting of 100 chains each with N_{cl} = 900 at 300 K. (a) Undeformed 3D configuration. (b) Undeformed plane configuration. (c) Plane configuration at a strain of 1.5. (color online)

The total number of carbons in the cluster N_{All} (all number of carbons in a cubic cell) is kept constant ($N_{All} = 7200$), while chain length, N_{cl} of polymer are varied from 6 to 900. The number of molecules N_{mol} (number of chains) changes accordingly from 1200 ($N_{cl} = 6$) to 8 ($N_{cl} = 900$). Each generated cluster is annealed for 120 ps so that the pressure and energy of the system becomes stable, keeping both the temperature T = 500 K and the pressure P = 1 atm in the *NPT* ensemble controlled by Berendsen's thermostat,[35] and barostat.[36] After the annealing process, the system is cooled down to the given temperature by the same *NPT* process. For each cooling simulation, the bulk density, thermal expansion coefficient, and glass-transition temperature T_g are calculated. In view of nonequilibrium MD simulations on uniaxial tension and compression tests, these initial structures are generated in $15 \times 15 \times 15$ nm^3 cubic space to accurately calculate the mechanical properties. The total number of carbons N_{All} in the cluster is kept constant (N_{All} = 90,000), while chain length, N_{cl} of

polymer are varied from 9 to 900. The number of molecules N_{mol} changes accordingly from 10,000 (N_{cl} = 9) to 100 (N_{cl} = 900). After a similar annealing process (220 ps) and then keeping the structures in the *NVT* ensemble (200 ps), uniaxial tension and compression tests are performed to obtain stress–strain response of the models with different chain length and temperature as well as strain rate in *NVT* ensemble.

All the MD simulations have been achieved using LAMMPS[37] software, while the initial cluster generation and post-processing was implemented in Fortran95 computer language by the authors.

III. RESULTS AND DISCUSSION

A. Bulk density and thermal expansion coefficients

The CG potentials of PE developed by Nielsen et al.[24] have been proved to give reasonable bulk densities compared with the experimental values[38] at 303 K temperature for short alkanes like $N_{cl} \leq 18$. The potentials, however, have not been validated to date for longer chain length usually found in bulk PE. The nonbonded pair potential between M-type beads, which are not considered in Nielsen et al.'s article,[24] plays an increasing role with the increase of chain length. Here, we adopt the nonbonded potentials by Shinoda et al.[34] (see Table I) with truncation radius r_c = 15 Å, and calculate the bulk density by MD for entangled PE up to N_{cl} = 600. The obtained bulk densities are in excellent agreement with Nielsen's results at 303 K for $N_{cl} \leq 18$, and with MC simulations[39] as well as Dee et al.'s[40] experimental results at 450 K for longer chain length in Figs. 2(a) and 2(b) (All of the differences are less than 5%.). In the latter case, Laso and Perpete[39] introduced a hyperbolic function to predict the bulk density by MC methods

$$\rho(N_{cl}, T, P) = \frac{\rho_{inf}(T, P) N_{cl}}{a_0(T, P) + N_{cl}} \quad , \qquad (1)$$

where $\rho_{inf}(T, P)$ denotes the density value at infinite N_{cl}, and a_0 (T, P) is a dimensionless constant describing the rate with which ρ increases with N_{cl} at the temperature and pressure conditions of the simulation.

Obviously, the difference between Eq. (1) and the present results is small (<5%) in Fig. 2(a) where ρ_{inf} (450 K, 1 atm) = 0.775 g/cm^3 and a_0(450 K, 1 atm) = 3.2 in Eq. (1).[39] Therefore, Eq. (1) can also predict the present results. To study which reason results in the relationship between ρ and N_{cl}, the following relationship is obvious in our cross-link-free cluster simulation

$$N_{bead} = N_{mol} + N_{bond} \quad , \qquad (2)$$

where N_{bond} is the number of bonds between CG beads, N_{bead} is the number of all CG beads, and N_{mol} is the number of chains.

Thus, the number of chain length can be written as

$$N_{c1} = 3N_{bead}/N_{mol} = 3N_{bead}/(N_{bead} - N_{bead}) \quad . \qquad (3)$$

Submitting Eq. (3) into Eq. (1) gives

$$\frac{1}{\rho(\frac{N_{bond}}{N_{bead}}, T, P)} = \frac{[3 + a_0(T,P)]}{3\rho_{inf}(T,P)} - \frac{a_0(T,P)}{3\rho_{inf}(T,P)} \frac{N_{bond}}{N_{bead}} \quad . \qquad (4)$$

Let $\frac{1}{\rho(\frac{N_{bond}}{N_{bead}},\ T,\ P)} = V, N_{bond}/N_{bead} = \xi$, and then Eq. (4) can be expressed as

$$V = \frac{(3 + a_0)}{3\rho_{inf}} - \frac{a_0}{3\rho_{inf}} \xi \quad . \qquad (5)$$

As shown in Eq. (5), we can find that ξ is a key parameter that dominates the bulk density of PE. It is interesting to find that Eq. (5) is a linear function and can be determined only using two points [see Fig. 2(c)]. As shown in Fig. 2(d), the ρ_{inf} and a_0 with different temperature at 1 atm pressure are calculated from Eq. (5) by fitting the present bulk densities. In general, the chain length $N_{cl} \geqslant 900$ is often taken as an infinite chain length.[39] It can also be found that the difference of bulk density between N_{cl} = 600 and N_{inf} is small (<8%) except for 500 K (12.3%) in Fig. 2(b). Therefore, we can approximately take N_{cl} = 600 as N_{inf} when the accuracy of density does not need to be high. Figures 2(a) and 2(d) show that the present results [ρ_{inf}(450 K, 1 atm) = 0.762 g/cm^3] are more accurate than those of the MC method [ρ_{inf}(450 K, 1 atm) = 0.775 g/cm^3] when compared with Dee et al.'s[40] experimental results [ρ_{inf}(450 K, 1 atm) = 0.766g/cm^3]. For practical application, the $\rho_{inf} = -4.829 \times 10^{-4}T + 0.9788$ and $a_0 = 7.881 \times 10^{-5}T^2 + 0.8186$ are both fitted using the least squares method. The previous analysis indicates that the present CG potential and bulk structure generated by the semicrystalline lattice method works satisfactorily and can be applied to the whole range of N_{cl}.

In this work, we have used the same bulk cubic cell and number of beads in the initial configuration but with different N_{cl}. The less the N_{cl} is the less the bonds and angles are in the unit cell, so the required energy to reach the same volume is smaller. That is to say, the shorter the N_{cl} the larger the volume is at the same temperature. Although the two types of bonds (Table I) consist of different potential parameters, the difference between them is small. Therefore, the potential energy for the system will be mainly determined by the total number of bonds for the given number of CG beads.

In this study, the volumetric thermal expansion coefficient is defined as[41]

$$\varepsilon_v = \frac{1}{V}\left(\frac{\partial V}{\partial T}\right)_p \quad , \qquad (6)$$

where T is the temperature, V is the volume, derivatives are taken at constant pressure p (Here p is 1 atm.).

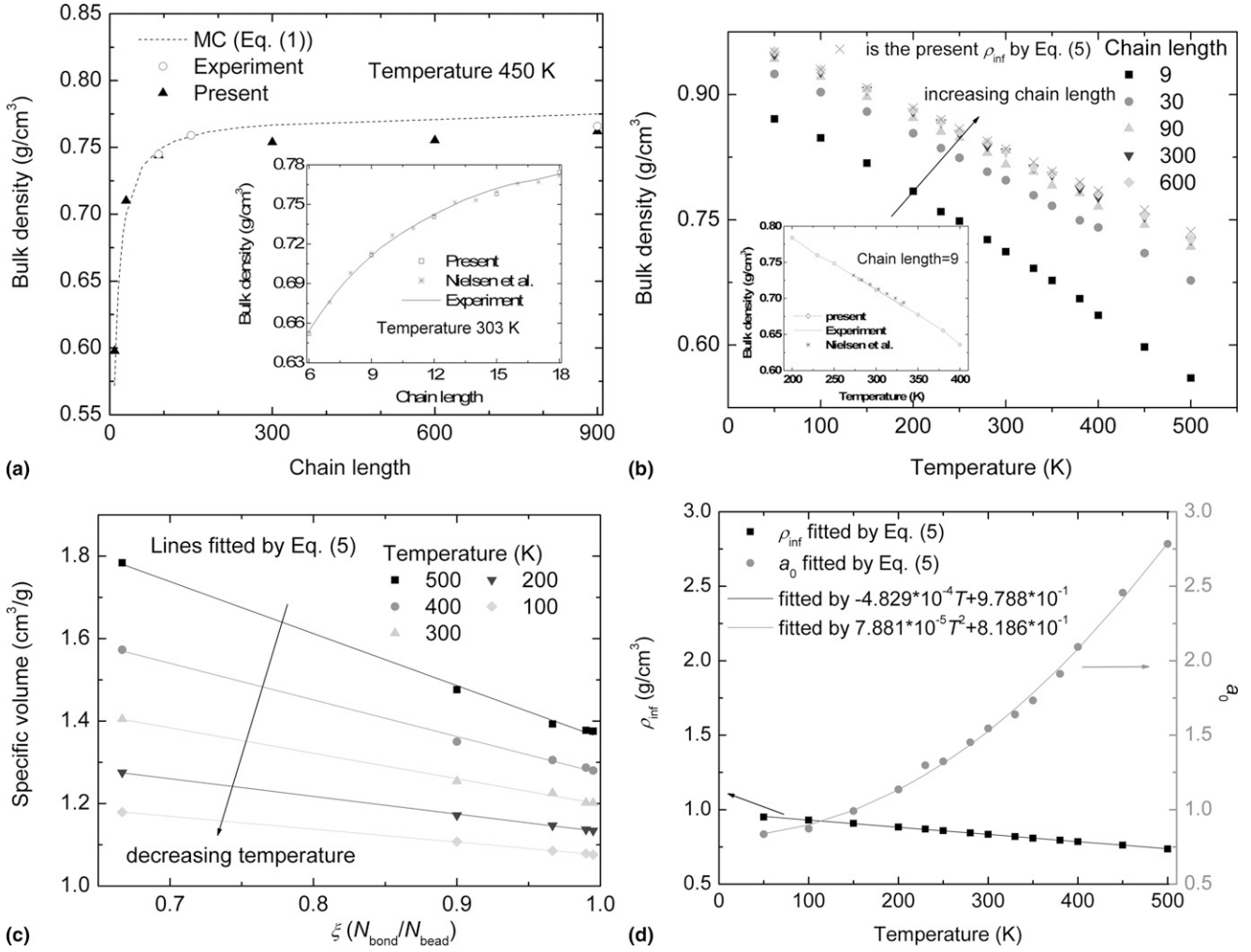

FIG. 2. Distribution of present bulk density with different chain length, temperature, and ξ. (a) Comparison of present bulk density with MC simulation results and Nielsen et al.'s experimental and computational results. (b) The variation of bulk density with different temperature and chain length (inset graph displays comparison of present bulk density with Nielsen's experimental and computational results for nonane). (c) Change of specific volume with ξ. (d) Variation of present bulk density ρ_{inf} (g/cm^3) and a_0 with different temperature at 1 atm pressure.

Submitting Eq. (5) into Eq. (6), we obtain

$$\alpha_v = \frac{1}{a_0}\frac{\partial a_0}{\partial T} - \frac{1}{\rho_{inf}}\frac{\partial \rho_{inf}}{\partial T} + \frac{\frac{3}{a_0^2}\frac{\partial a_0}{\partial T}}{\xi - \left(1 + \frac{3}{a_0}\right)} \quad . \qquad (7)$$

Because ρ_{inf} and a_0 are independent of ξ, Eq. (7) can be further simplified to

$$\alpha_v = A + \frac{B}{\xi - C} \quad , \qquad (8)$$

where the parameters of A, B, and C are only dependent on the temperature. For the same temperature, these three parameters are independent of chain length. Therefore, α_v can be easily obtained from Eq. (7) if the functions of ρ_{inf} and a_0 are given.

Figure 3(a) plots the change of normalized volume with temperature. Figure 3(b) plots the distributions of α_v with ξ. It can be seen that α_v of N_{cl} = 9 is 1.5 times more than that of N_{cl} = 600. Equation (8) shows that α_v is a linear rational function of ξ.

B. Glass-transition temperature (T_g)

T_g is one of the most important single descriptors of different amorphous polymers because its value determines the type of application.[23] The ability to predict T_g from the chemical structure of the polymer repeat unit would be of great value in the selection and design of new materials.

Capaldi et al.[23] reported the pressure dependence of T_g using the UA MD method, while the effect N_{cl} was not focused. Here, the effect of N_{cl} on T_g are presented by specific volume versus temperature (V–T) curves in Fig. 4. At different values of N_{cl} the curves are fitted by two straight lines using the least squares fit. The intersections of these two lines are marked as T_g [see Fig. 4(b)]. It can be found that the T_g values are from 250 to 310 K

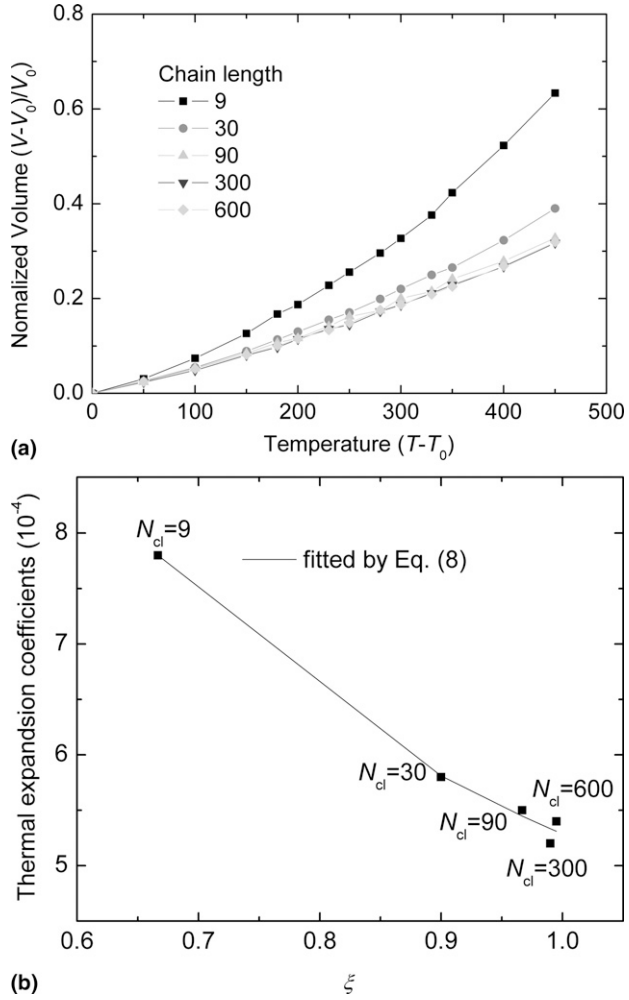

FIG. 3. Volumetric thermal expansion coefficients with different chain length and ξ. (a) The normalized volume versus temperature (V_0 is the corresponding volume for T_0 = 50 K). (b) The change of thermal expansion coefficients with different chain length and ξ.

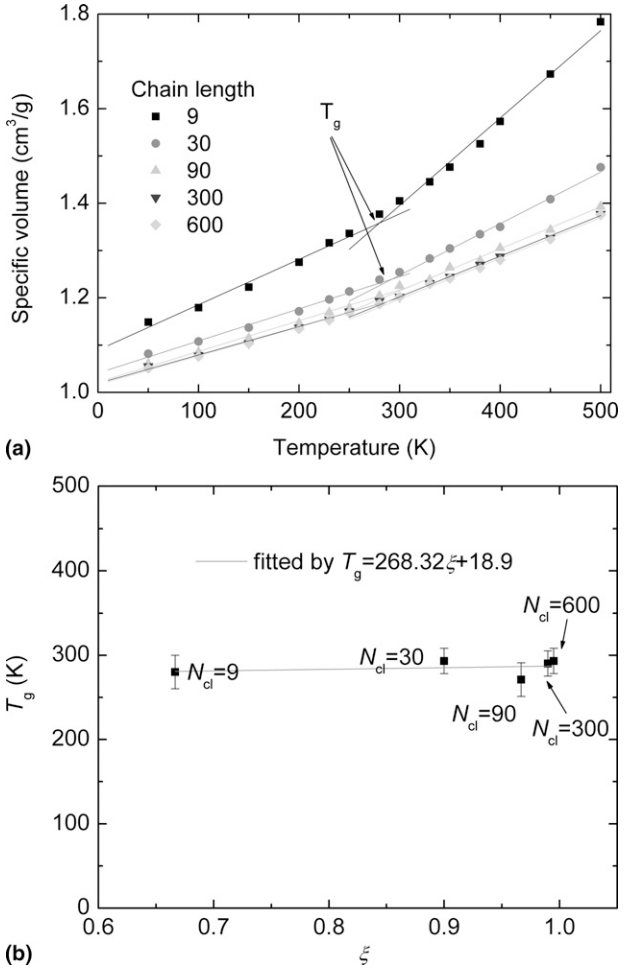

FIG. 4. Variation of specific volume and T_g with different temperature and chain length. (a) Variation of specific volume with different temperature. (b) Variation of T_g with different chain length.

for different N_{cl}, which are close to Capaldi et al.'s results (280 ± 32 K)[23] and experimental results (~250 K).[42]

The present values of T_g with different chain length is fitted by a linear function in Fig. 4. It can be seen that T_g changes weakly with ξ, and it does not seem to be sensitive to chain length. Here, the T_g is fitted by a linear equation $T_g = 268.32\xi + 18.9$ using the least squares method. From Gee and Boyd's[43] analysis, we know that the torsional potential has some effect on the T_g values. In this work, it is not considered in the present CG method, which is one of the possible reasons that the present T_g is not sensitive to chain length. In addition, slow structural relaxations can still occur even below such a temperature and detectable relaxations cease altogether only at somewhat lower temperatures.[44] Signorini et al.[45] have pointed out that in the small molecule system studied by an MD simulation, the true transition temperature lies some 100° below the temperature determined from the break in the *V–T* curves. Therefore, the true T_g is from 190 to 290 K with different N_{cl}, which is in good agreement with the available computational and experimental data.[23,42]

C. Mechanical properties

Some mechanical properties of PE under uniaxial compression have been reported using the UA MD method,[23] while the effect of N_{cl} and temperature was not considered. In this work, we use the CG MD method to study the effect of N_{cl}, temperature and strain rate on the stress–strain curves and Young's modulus under tension and compression.

The strain is measured in the following based on the dimensions of the periodic cubic cell:

$$\varepsilon_y = \frac{y - y_0}{y_0} \quad , \tag{9}$$

where y is the current length of the cell, y_0 is the initial length of the cell before the commencement of deformation. Because our interest is to study the effect of temperature and N_{cl} on the stress–strain curves under

uniaxial tension and compression, the *y*-axial direction loading is chosen in this work (see Fig. 1).

The pressure on each face of the simulation cell is given as the normal tensor component of the virial stress,

$$\sigma_v = \frac{1}{V}\left(\sum_{i=1}^{N_{\text{bead}}} m_i v_i v_i - \sum_{i=1, j<i}^{N_{\text{bead}}} r_{ij}\frac{\partial U_{ij}}{\partial r_{ij}}\right) \quad , \qquad (10)$$

where V is the current volume of the periodic unit cell, m_i is the mass of atom i, v_i is the velocity, r_{ij} is the displacement vector between the atoms i and j, and U_{ij} is the potential energy between atoms i and j.

To facilitate the plot of the curves under both tension and compression, we define that compressive stress is negative and tensile stress is positive. In fact, it is often difficult to precisely define yielding due to the wide variety of stress–strain curves exhibited by real materials.[28] In this work, the yield strain will be given by observing stress–strain curves from linear elastic response to a nonlinear transition. Figure 5 plots the change of stress–strain curves with temperature. It can be seen that the curves have a softening process under tension at 100 and 200 K, while the softening does not occur at temperatures higher than 300 K. It is possible that the softening process disappears at $T > T_g$ because PE behaves like a liquid. It indicates that T_g is between 200 and 300 K, which is in good agreement with our calculated T_g. From the stress–strain curves, the tensile and compressive yield strains are taken 0.1 and 0.15, respectively. The absolute value of yield stress decreases with the increase of temperature. The tensile and compressive yield stress at 100 K is about 4∼7 times that at 500 K. To investigate the behavior at small strain, the cell is deformed with a slow strain rate 3×10^9 1/s and the stresses are taken as average values every 5000 time steps in Fig. 5(b) in which the corresponding deviations are also plotted. The tensile and compressive yield strain is about at absolute value of strain 0.15, and intrinsic strain softening then occurs at the strain 0.15∼0.25 in Fig. 5(b). When the strain is larger than 0.25, the strain hardening occurs. These phenomena can also be seen in the available experimental results.[10,45] The process from tension to compression is very smooth, and the Young's moduli are then obtained using $d\sigma/d\mathrm{E}$ as plotted in Fig. 5(b). It can be seen that the Young's modulus at 100 K is about 10 times that at 500 K, and the Young's modulus at 300 K is 195 MPa, which is close to the experimental result (200 MPa).

As shown in Fig. 6, the cell is deformed in the *y*-axis direction under uniaxial tension and compression at a constant strain rate of 3×10^{10} 1/s. The stress increases

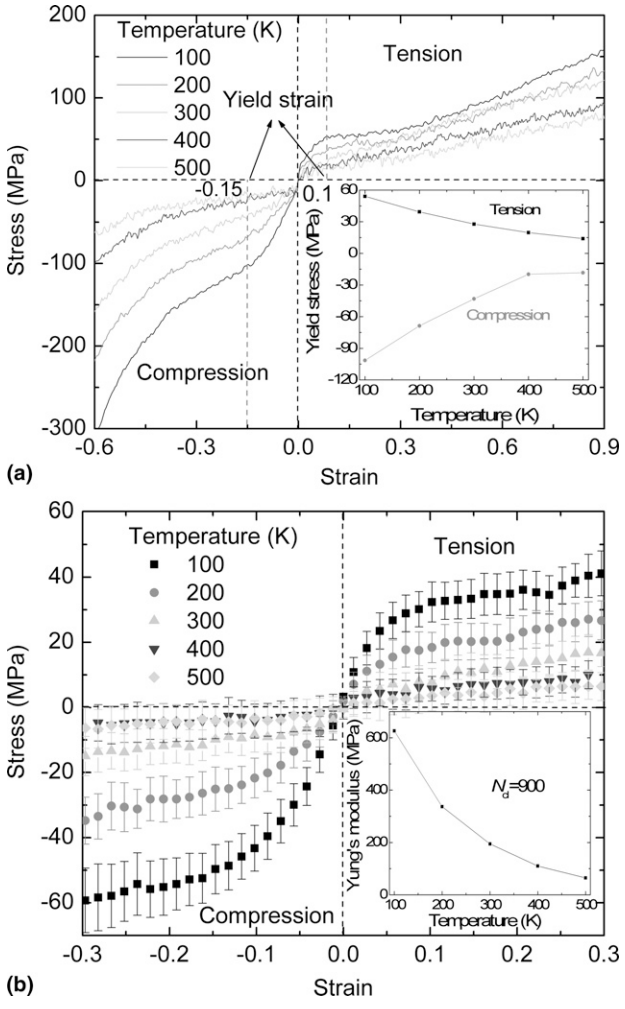

FIG. 5. Stress–strain curves under tension and compression with different temperature at N_{cl} = 900. (a) Stress–strain curves under tension and compression with different temperature (strain rate = 3×10^{10} 1/s) (inset graph displays the change of yield stresses with different temperature). (b) Stress–strain curves under tension and compression with different temperature (strain rate = 3×10^9 1/s) (inset graph displays the change of Young's moduli with a different temperature).

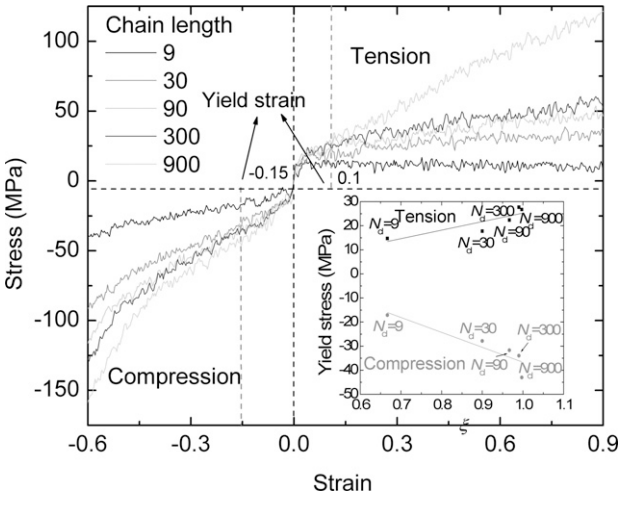

FIG. 6. Stress–strain curves under tension and compression with different chain length at 300 K (inset graph displays the change of yield stresses with different chain length and ξ).

with the increase of chain length at a given strain. To facilitate the comparison, the tensile and compressive yield strains are also taken 0.1 and −0.15, respectively. The two types of yield stress (absolute value) almost linearly increase with the increase of ξ. Therefore, it indicates that ξ plays an important role in the mechanical properties.

Figure 7 plots the stress–strain curves and yield stresses with different strain rates. It can be found that the stresses and corresponding yield stresses increase with the increase of strain rate. It is interesting to find that the difference at 3×10^{10} and 1×10^{10} 1/s under compression is small, while the yield stress under compression at 1×10^{11} is approximately 9 times 1×10^{10} 1/s. The yield stress under tension at 1×10^{11} 1/s is about 4.5 times that at 1×10^{10} 1/s. This clearly indicates that the PE has

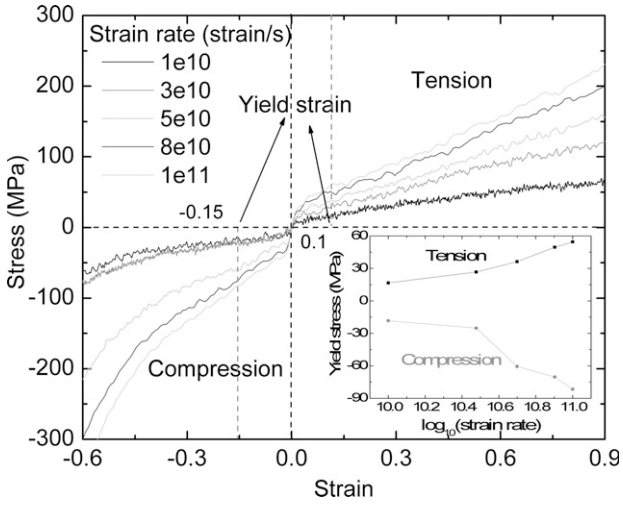

FIG. 7. Stress–strain curves and yield stresses under tension and compression with different strain rate at N_{cl} = 900 and 300 K (inset graph displays the change of yield stresses with different temperature).

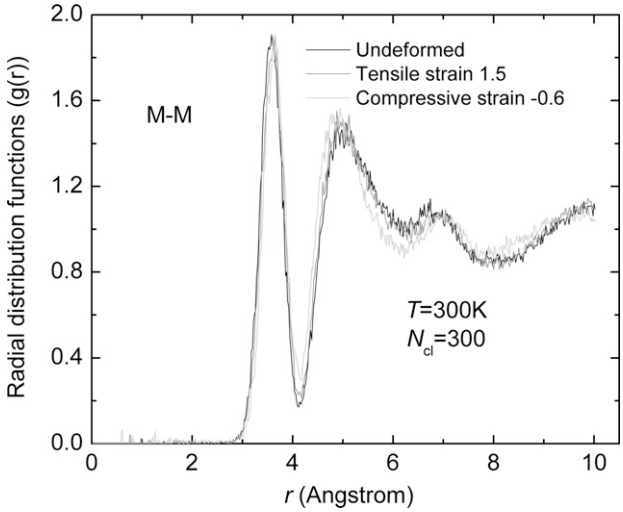

FIG. 8. Coarse grain radial distribution functions [$g(r)$] for M-M units of N_{cl} = 300 under undeformed structure, tensile strain, and compressive strain.

obvious viscoelastic property, which can also be reflected from the experimental results.[46–48] For the same tensile or compressive strain, the larger the velocity, the shorter required time is, and the stress should then be higher based on the Ferry's theory[49] and the coupling model of Plazek and Ngai.[48,50]

To check the structure under compression and tension, Fig. 8 plots the radial distribution function $g(r)$ of middle-middle (M-M) units of N_{cl} = 300 under the undeformed structure, tensile strain (1.5), and compressive strain (−0.6). The first peaks for the three conditions are at 3.58, 3.56, and 3.62 Å, respectively. Obviously, the first peak for undeformed structure corresponds to the first neighbor distance in cubic diamond (3.64 Å). The second and third peaks are at 4.88, 4.88, and 4.94 Å as well as at 6.70, 7.04, and 6.92 Å, respectively. It is clear that the slight discrepancy in location reflects the strain in the bulk PE.

IV. CONCLUSIONS

By extensive coarse-grained molecular dynamics simulations, we studied the bulk density, thermal expansion coefficient, T_g, and mechanical behaviors of bulk PE under tension and compression with different N_{cl} and temperatures. The following conclusions can be drawn:

(1) The specific volume and the thermal expansion coefficient (α_v) decrease with the increase of N_{cl}. α_v has shown to be a linear rational function of ξ. The calculated T_g values with different N_{cl} varied from 250 to 310 K. Finally, a formula is proposed to estimate α_v as a function of chain length.

(2) The stress and corresponding compressive and tensional yield stresses decrease with the increase of temperature and the decrease of strain rate as well as chain length. The two types of yield stresses (absolute values) almost linearly increase with the increase of ξ. Young's modulus decreases with increasing temperature and its value at 100 K is about 10 times that of 500 K.

(3) It seems that ξ is the key parameter, which dominates the mechanical and physical properties of the present CG-modeled linear PE.

ACKNOWLEDGMENTS

Financial support for the work from the Research Council of Norway and our industrial partner Conpart AS (www.conpart.no) via the NANOMAT KMB (MS2MP) Project "From Molecular Structures to Mechanical Properties: Multiscale Modelling for Ugelstad Particles" is appreciated.

REFERENCES

1. H. Takeuchi and R.J. Roe: Molecular dynamics simulation of local chain motion in bulk amorphous polymers. I. Dynamics above the glass transition. *J. Chem. Phys.* **94,** 7446 (1991).

2. P.V.K. Pant, J. Han, G.D. Smith, and R.H. Boyd: A molecular dynamics simulation of polyethylene. *J. Chem. Phys.* **99,** 597 (1993).
3. R.H. Boyd, R.H. Gee, J. Han, and Y. Jin: Conformational dynamics in bulk polyethylene: A molecular dynamics simulation study. *J. Chem. Phys.* **101,** 788 (1994).
4. J.R. Hanscomb and Y. Kaahwa: High-temperature electrical conduction in polyethylene-terephthalate. II. Analysis. *J. Phys. D: Appl. Phys.* **12,** 579 (1979).
5. J.R. Hanscomb and Y. Kaahwa: High-field transient conduction in PET in the microsecond-millisecond time range. *J. Phys. D: Appl. Phys.* **11,** 725 (1978).
6. A.M. Donald and E.J. Kramer: Effect of strain history on craze microstructure. *Polymer (Guildf.)* **23,** 457 (1982).
7. A.M. Donald, E.J. Kramer and R.A. Bubeck: The entanglement network and craze micromechanics in glassy polymers. *J. Polym. Sci., Part B: Polym. Phys.* **20,** 1129 (1982).
8. C. G'Sell, J.M. Hiver, A. Dahouin and A. Souahi: Video-controlled tensile testing of polymers and metals beyond the necking point. *J. Mater. Sci.* **27,** 5031 (1992).
9. E.M. Arruda and M.C. Boyce: Evolution of plastic anisotropy in amorphous polymers during finite straining. *Int. J. Plast.* **9,** 697 (1993).
10. M.C. Boyce, E.M. Arruda, and R. Jayachandran: The large strain compression, tension, and simple shear of polycarbonate. *Polym. Eng. Sci.* **34,** 716 (1994).
11. H.G.H. van Melick, L.E. Govaert, and H.E.H. Meijer: On the origin of strain hardening in glassy polymers. *Polymer (Guildf.)* **44,** 2493 (2003).
12. J.Y. He, Z.L. Zhang, M. Midttun, G. Fonnum, G.I. Modahl, H. Kristiansen, and K. Redford: Size effect on mechanical properties of micron-sized PS-DVB polymer particles. *Polymer (Guildf.)* **49,** 3993 (2008).
13. H. Eyring: Viscosity, plasticity, and diffusion as examples of absolute reaction rates. *J. Chem. Phys.* **4,** 283 (1936).
14. R.E. Robertson: Theory for the plasticity of glassy polymers. *J. Chem. Phys.* **44,** 3950 (1966).
15. A.S. Argon: A theory for the low-temperature plastic deformation of glassy polymers. *Philos. Mag.* **28,** 839 (1973).
16. P.D. Wu and E. van der Giessen: On improved network models for rubber elasticity and their applications to orientation in glassy polymers. *J. Mech. Phys. Solids* **41,** 427 (1993).
17. D. Riby and R.J. Roe: Molecular dynamics simulation of polymer liquid and glass. II. Short range order and orientation correlation. *J. Chem. Phys.* **89,** 5280 (1988).
18. P.G. Whitten and H.R. Brown: Polymer entanglement density and its influence on interfacial friction. *Phys. Rev. E: Stat. Nonlinear Soft Matter Phys.* **76,** 026101 (2007).
19. A.V. Lyulin, N.K. Balabaev, and M.A.J. Michels: Correlated segmental dynamics in amorphous atactic polystyrene: A molecular dynamics simulation study. *Macromolecules* **35,** 9595 (2002).
20. N.F.A. van der Vegt, W.J. Briels, M. Wessling, and H. Strathmann: Free energy calculations of small molecules in dense amorphous polymers. Effect of the initial guess configuration in molecular dynamics studies. *J. Chem. Phys.* **105,** 8849 (1996).
21. R.M. Sok and H.J.C. Berendsen: Time-dependent self-diffusion in a semidilute suspension of Brownian particles. *J. Chem. Phys.* **96,** 4699 (1992).
22. F. Zhang: Molecular-dynamics simulation of solitary waves in polyethylene. *Phys. Rev. E: Stat. Phys. Plasmas Fluids Relat. Interdisciplin. Top.* **56,** 6077 (1997).
23. F.M. Capaldi, M.C. Boyce, and G.C. Rutledge: Molecular response of a glassy polymer to active deformation. *Polymer (Guildf.)* **45,** 1391 (2004).
24. S. Nielsen, C.F. Lopez, G. Srinivas, and M.L. Klein: A coarse grain model for *n*-alkanes parameterized from surface tension data. *J. Chem. Phys.* **119,** 7043 (2003).
25. A.A. Louis: Beware of density dependent pair potentials. *J. Phys. Condens. Matter* **14,** 9187 (2002).
26. R.L.C. Akkermans and W.J. Briels: A structure-based coarse-grained model for polymer melts. *J. Chem. Phys.* **114,** 1020 (2001).
27. M. Zhang and F. Müller-Plathe: The Soret effect in dilute polymer solutions: Influence of chain length, chain stiffness and solvent quality. *J. Chem. Phys.* **125,** 124903 (2006).
28. A. Di Matteo, F. Müller-Plathe, and G. Milano: From mesoscale back to atomistic models: A fast reverse-mapping procedure for vinyl polymer chains. *J. Phys. Chem. B* **111,** 2765 (2007).
29. T. Terao, E. Lussetti, and F. Müller-Plathe: Non-equilibrium molecular dynamics methods for computing the thermal conductivity: Application to amorphous polymers. *Phys. Rev. E: Stat. Nonlinear Soft Matter Phys.* **75,** 057701 (2007).
30. M. Fermeglia and S. Pricl: Multiscale modeling for polymer systems of industrial interest. *Prog. Org. Coat.* **58,** 187 (2007).
31. S. Pricl, M. Fermeglia, M. Ferrone, and A. Asquini: Scaling properties in the molecular structure of three-dimensional, nanosized phenylene-based dendrimers as studied by atomistic molecular dynamics simulations. *Carbon* **41,** 2269 (2003).
32. C.D. Wick and D.N. Theodorou: Connectivity-altering Monte Carlo simulations of the end group effects on volumetric properties for poly(ethylene oxide). *Macromolecules* **37,** 7026 (2004).
33. J.L. Faulon: Stochastic generator of chemical structure. (4) Building polymeric systems with specified properties. *J. Comput. Chem.* **22,** 580 (2001).
34. W. Shinoda, R. Devane, and M.L. Klein: Multi-property fitting and parameterization of a coarse grained model for aqueous surfactants. *Mol. Simul.* **33,** 27 (2007).
35. H.J.C. Beredsen, J.P.M. Postma, W.F. van Gunsteren, A. Dinola, and J.R. Haak: Molecular dynamics with coupling to an external bath. *J. Chem. Phys.* **81,** 3684 (1984).
36. H. Takeuchi and R.J. Roe: Molecular dynamics simulation of local chain motion in bulk amorphous polymers. II. Dynamics at glass transition. *J. Chem. Phys.* **94,** 7458 (1991).
37. S. Plimpton: Fast parallel algorithms for short-range molecular dynamics. *J. Comput. Phys.* **117,** 1 (1995).
38. M.M. Rudek, J.A. Fisk, V.M. Chakarov, and J.L. Katz: Condensation of a supersaturated vapor. XII. The homogeneous nucleation of the n-alkanes. *J. Chem. Phys.* **105,** 4707 (1996).
39. M. Laso and E.A. Perpete: *Multiscale Modelling of Polymer Properties* (Elsevier, Amsterdam, The Netherlands, 2006), pp. 31–45.
40. G.T. Dee,T. Ougizawa, and D.J. Walsh: The pressure-volume-temperature properties of polyethylene, poly(dimethyl siloxane), poly(ethylene glycol) and poly(propylene glycol) as a function of molecular weight. *Polymer (Guildf.)* **33,** 3462 (1992).
41. D.L. Turcotte and G. Schubert: *Geodynamics*, 2nd ed. (Cambridge University Press, Cambridge, 2002).
42. J. Han, R.H. Gee, and R.H. Boyd: Glass transition temperatures of polymers from molecular dynamics simulations. *Macromolecules* **27,** 7781 (1994).
43. R.H. Gee and R.H. Boyd: The role of the torsional potential in relaxation dynamics: A molecular dynamics study of polyethylene. *Comput. Theor. Polym. Sci.* **8,** 93 (1998).
44. C.A. Angell, J.H.R. Clarke, and L.V. Woodcock: *Advances in Chemical Physics*, Vol. 48, edited by I. Prigogine and S.A. Rice (Wiley, New York, 1981), p. 397.
45. F. Signorini, J.L. Barrat, and M.L. Klein: Structural relaxation and dynamical correlations in a molten state near the liquid–glass transition: A molecular dynamics study. *J. Chem. Phys.* **92,** 1294 (1990).